ASSESSING ATMOSPHERIC THERMAL FORCING FROM SURFACE PRESSURE DATA: SEPARATING THERMAL TIDES AND LOCAL TOPOGRAPHIC INFLUENCE

R. J. Wilson, *Geophysical Fluid Dynamics Laboratory, Princeton, NJ, USA (John.Wilson@noaa.gov)*, **J. M. Murphy,** *New Mexico State University, Las Cruces, USA*., **D. Tyler**, *Oregon State University, Corvallis, OR, USA*.

Overview: The evolving distribution of radiatively active dust and water ice clouds plays a major role in modulating the seasonal and interannual variation in the thermal forcing of the Martian atmosphere, and thus the resulting intensity of the circulation. Thermal tides are the global-scale atmospheric response to the diurnally varying thermal forcing, due to aerosol heating within the atmosphere and radiative and convective heat transfer from the surface. The global tide includes westward propagating (sun-synchronous) waves driven in response to solar heating, as well as nonmigrating waves that result from zonal variations in the thermotidal forcing that are caused by variations in the surface (the topography and surface thermal properties) and the distribution of aerosols (dust and water ice clouds). The migrating tides are of particular interest, since they tend to be directly responsive to the aerosol distribution. However, distinguishing these tides from the mix of additional nonmigrating tides is difficult with only a limited number of surface observations.

We utilize a very high resolution Mars Global Circulation Model (MGCM) to simulate diurnal variability at scales ranging from craters to the planetary scale, thus distinguishing the pressure signature of local topographically driven circulations from that of the global tide. We define the latter as that resulting from a reconstruction of surface pressure using a compact set of tide modes derived from a space-time analysis of suitably normalized simulated surface pressure. This field includes the migrating tides, resonantly enhanced Kelvin waves and a small set of additional nonmigrating tides. The remaining residual pressure field is found to be highly localized and clearly associated with smaller-scale topographic features (such as craters), while the thermal tide reflects the effect of forcing at much larger scales. With this approach, it is possible to isolate the influence of local topographic circulations on the diurnal variation of surface pressure from that of the global thermal tide. Importantly, this enables the comparison of surface pressure observations at different lander sites with the global tide constructed from model results. We illustrate the value of this approach by comparing simulated surface pressure tide results from the LMD Mars Climate Database to those observed at the Mars Science Laboratory (MSL) and Viking Lander 1 (VL1) sites. The LMD model includes a state-of-the-art representation of radiatively active dust and water ice aerosols, and this provides an opportunity to investigate the impact of the aerosol distribution on the tides.

Thermal tides and aerosol: An observed tide harmonic, S_n, at a lander site represents the sum over all zonal wavenumbers, including the corresponding migrating component and additional eastward and westward propagating nonmigrating components. Migrating tides include DW1, SW2, TW3, QW4, and HW6, respectively for the westward propagating diurnal, semidiurnal, terdiurnal, quad-diurnal and hexadiurnal migrating tides. The most prominent nonmigrating tides are the resonantly enhanced, eastward propagating diurnal and semidiurnal Kelvin waves (DE1 and SE2). Model simulations suggest that the spatial distributions of diurnal and semidiurnal variability are dominated by the corresponding migrating tides and two resonantly enhanced eastward propagating Kelvin waves [*Wilson and Hamilton*, 1996; *Guzewich et al*., 2016]. This is illustrated in Fig. 1, where the seasonal variation of the equatorial amplitude of selected tide modes in MGCM simulations is shown for a specified uniform visible dust column opacity varying from zero to 1.5. The modes shown are the dominant contributions to pressure variability in their respective frequencies. The migrating tides (DW1, SW2, QW4 and HW6) exhibit monotonically increasing relationships between amplitude and aerosol forcing. QW4 and HW6 show a very pronounced seasonal variation, with maxima in the two equinoctial seasons, in agreement with the MSL and VL1 observations. DW1 shows a particularly prominent clear-sky tide response, which is due to forcing by sensible and radiative heat exchange with the surface and boundary layer turbulent mixing.

There is roughly a linear relationship between the SW2 amplitude and the dust column optical depth, which makes this mode an effective proxy for globally integrated thermal forcing. The simulated phases of SW2, QW4 and HW6 are respectively about 0900, 0200 and 0400 LT, in good agreement with both MSL and VL1 observations. The seasonal variation of the resonantly-enhanced Kelvin waves (DE1 and SE2) show a strong preference for the two solstice seasons, with a clear emphasis on the L_s = 90° season. These two modes contribute to significant zonal modulation of the S_1 and S_2, respectively [*Wilson and Hamilton*, 1996; *Guzewich et al*., 2016], which suggests that the ability to isolate key migrating tides offers an important opportunity

to constrain boundary layer and aerosol thermal forcing.

There now exists an extended record of surface pressure observations at two locations in the Martian tropics, as provided by the Rover Environmental Monitoring Station (REMS) aboard the MSL rover Curiosity in Gale crater (4.5°S, 137°E) and from VL1 (22.5°N, 312°E). The surface pressure records from MSL and VL1 are currently the only surface-based observations available for evaluating and validating atmospheric models. The high degree of reproducibility of the Viking tide record over 4 Mars years (MY12-15) in the aphelion season (L_s=0-135°), the reproducibility of 2 years of MSL observations, and the same reproducibility in Thermal Emission Spectrometer (TES) and Mars Climate Sounder (MCS) atmospheric temperatures in this season, all suggest that the atmospheric state observed by Viking during the aphelion season is likely the same as that seen by MSL. To the extent that this holds true, the two surface pressure records can be used as the basis for a two-station network. A better understanding of the global and local scale influences on the diurnal variability of surface pressure is critical for detailed comparisons between atmospheric models and observations. A network would be a most effective way to accomplish this.

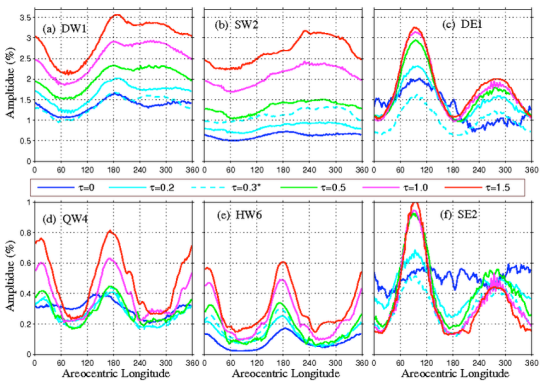

Figure 1. (a) Simulated seasonal variation of equatorial DW1 for 5 values of uniformly mixed dust with specified column dust opacity (τ = 0.0, 0.2, 0.5, 1.0, 1.5). An additional case (τ =0.3*, dashed curve) includes a detached dust layer that contributes an additional 0.1 unit of column opacity. (b) SW2. (c) DE1. (d) QW4. (e) HW6. (f) SE2.

The location of MSL within Gale crater has motivated investigations into how to best interpret the observed diurnal variations in surface pressure, and their seasonal dependence in terms of changes in the planetary-scale thermal forcing versus the local crater-scale forcing. The role of topographic circulations on the surface pressure cycle within craters has been explored by *Tyler and Barnes* [2013, 2015], who found that a sizable part of the diurnal surface pressure variation is caused by a crater circulation.

MGCMs include parameterizations that yield a thermal forcing field from distributions of dust and water ice clouds. Simulated atmospheric temperature and surface pressure are then obtained consistently as the atmosphere responds to the thermal forcing. The extent to which the simulated fields correspond to observations provides insight into how well the thermal forcing field is represented. It has become evident that radiative forcing by water ice clouds contributes significantly to the thermal balance particularly in the aphelion season [*Wilson et al*., 2008; *Madeleine et al*., 2012; *Wilson et al*., 2014], although details are still poorly constrained. Another poorly constrained issue is the effect of vertical variation of dust (detached dust layers) on thermal forcing.

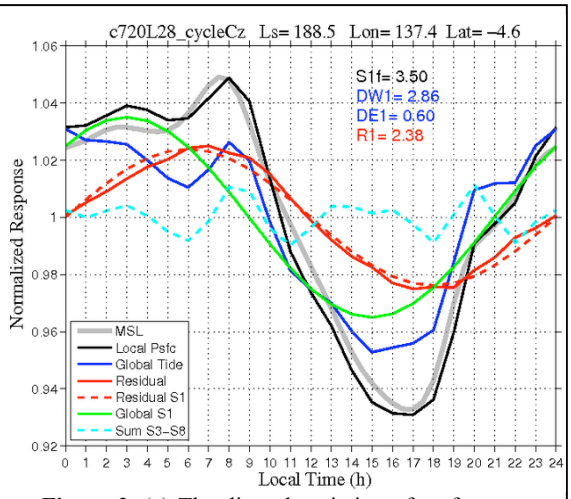

Figure 2. (a) The diurnal variation of surface pressure within Gale crater is shown in black. The observed variation by MSL is shown in gray. The diurnal variation reconstructed from the planetary tide components is shown in blue and the green curve is the diurnal component of this global tide. The residual pressure variation is shown in red and the dotted red curve is the diurnal component. The dashed cyan curve is the sum of the higher frequency tide harmonics.

Very High Resolution Simulations: The GFDL MGCM uses a finite volume dynamical core in a cubed-sphere geometry, which enables very high-resolution simulations on a relatively uniform grid. We have performed such simulations (C180, C360, and C720) to examine the local and global-scale surface pressure responses. The C720 simulation has a resolution of 0.125° x 0.125° (~7.5 km). The highest resolution simulations (C360 and C720) are run for only relatively short periods at present (~20-30 sols), and make use of surface temperature and CO_2 gas and ice fields taken from annual C180 simulations.

We can therefore define the planetary-scale tide as the reconstructed surface pressure field using a relatively compact set of the planetary-scale tide modes that have been isolated by a space-time decomposition of the high resolution surface pressure field sampled at hourly intervals. We include all migrating tides out to σ= 8, the corresponding Kelvin modes and a small set of diurnal and semidiurnal period harmonics with zonal wavelengths less than 6. We define the residual diurnal surface pressure variation as the difference between the local diurnal

pressure signal and the reconstructed planetary-scale tide.

The simulated diurnal surface pressure variation at the MSL site within Gale crater is shown in Fig. 2 for L_s = 188°. The model variation is in very good agreement with the observed signal. The surface pressure variation due to the planetary-scale thermal tide and the resulting residual pressure signal are also shown in Fig. 2. The residual is strongly dominated by the diurnal harmonic, which can be characterized with an amplitude and phase. In this case, the residual amplitude is ~2.4% of the diurnal mean pressure and the phase is ~0600 LT. A crater circulation is the logical explanation for the sizable residual, which contributes substantially to the total signal. The higher frequency modes S_4 and S_6, are dominated by QW4 and HW6 in the simulation. The constructive superposition of QW4 and HW6 at 0800 and 2000 LT is consistent with the observations at MSL, Pathfinder, and VL1.

Tyler and Barnes [2015] carried out idealized modeling of crater circulations in the absense of thermal tides. Their intent was to isolate the impact of crater-induced slope winds, and the resulting circulation, on surface pressure and the depth of the convectibe boundary layer (CBL) within a crater. For a Gale crater analog at the season of MSL landing, they found a diurnal-period response with an amplitude of ~2%. Experimenting with many idealized craters, they found that the actual enhancement is highly sensitive to the depth of the crater. Here, the phase of the residual is consistent with the net effect of a slope wind circulation, where the ~2.4% amplitude is dependent on the specific representation of Gale crater and the season of the simulation.

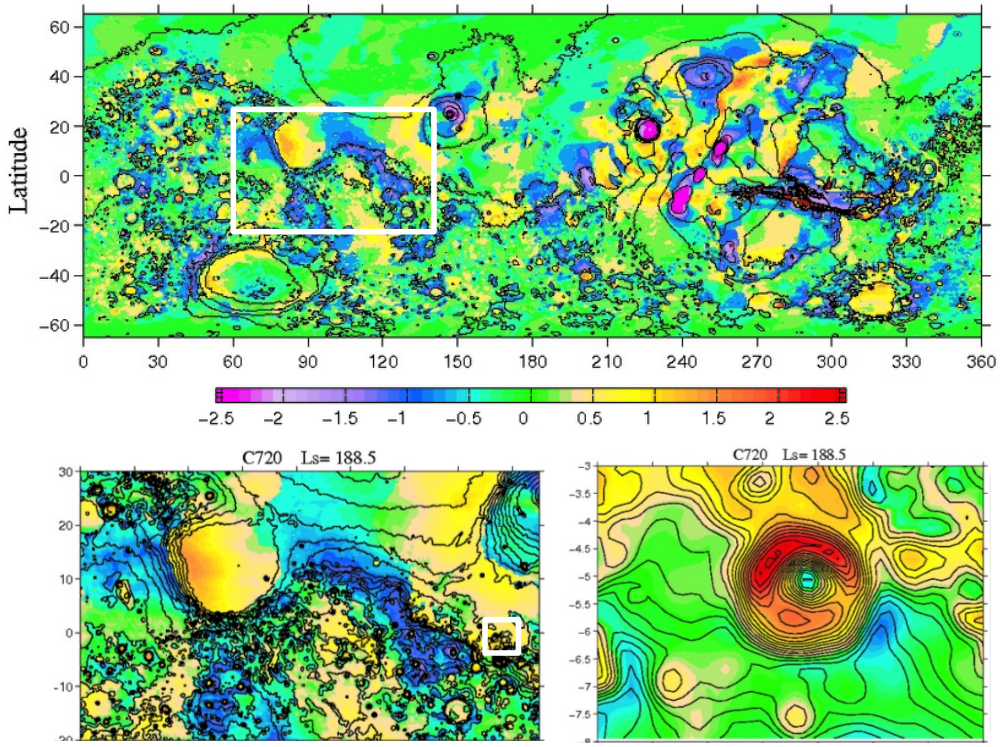

Figure 3. (a) The amplitude of the diurnal component of the residual pressure at L_s=188° as a percentage of the diurnal mean pressure. Positive values indicate regions where the phase is earlier than 1200 LT while negative values correspond to regions with the amplitude maximum after 1200 LT. Topography is contoured at intervals of 2 km. (b) Zoomed view of the residual pressure signal with topography shown at 0.5 km intervals. (c) A zoomed view of Gale crater with topography at 0.25 km intervals.

The amplitudes and phases of the various diurnal harmonics of the residual pressure field can be plotted for each location on the planet. In general, the diurnal harmonic is the most prominent component of the residual field. Maps of the amplitude of the diurnal harmonic of the residual pressure response are shown in Fig. 3. The amplitude is displayed as negative in regions where the phase peaks after midday (1200 LT), while positive amplitudes show regions where the maximum pressure response occurs before noon. There is a clear association of early phase response (typically ~0400-0800 LT) within craters, channels, and basins, while the late phase response is seen in regions of elevated terrain adjacent to steep slopes. These late-phase instances are evidently due to the strong slope wind effects that are prominent in mesoscale model results over such topography, as can be seen quite clearly near the peaks of the various steep volcanoes and in the highlands forming the western rims of Hellas basin and Isidis Planitia. The zoomed view in Fig. 3 provides greater detail, revealing an enhanced diurnal pressure response within Isidis Planitia and within all the craters. A further zoom shows the amplitude re-

sponse in the vicinity of Gale crater, a result that is in very good agreement with the enhancement of the diurnal pressure range found by *Tyler and Barnes* [2013, 2015].

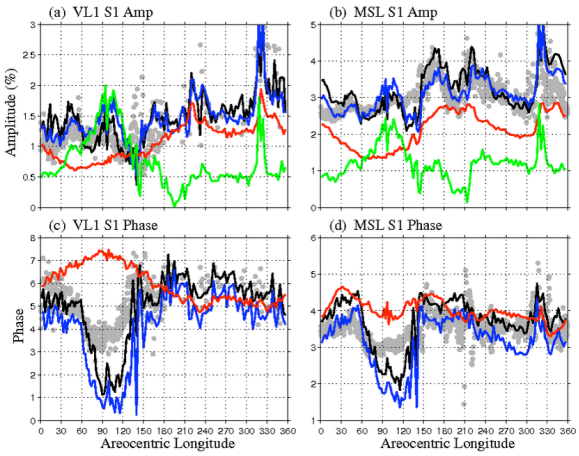

Figure 4. Black curves show the simulated amplitude (top row) and phase (bottom row) of S_1 at VL1 and MSL using the LMD MY26 simulation. The VL1 and "corrected" MSL observations are shown in grey. Red curves show the migrating tide (DW1) contributions to S_1 while green curves show the near-resonant Kelvin wave contributions (DE1). The blue curves show the reconstruction of S_1 based on DW1 and DE1.

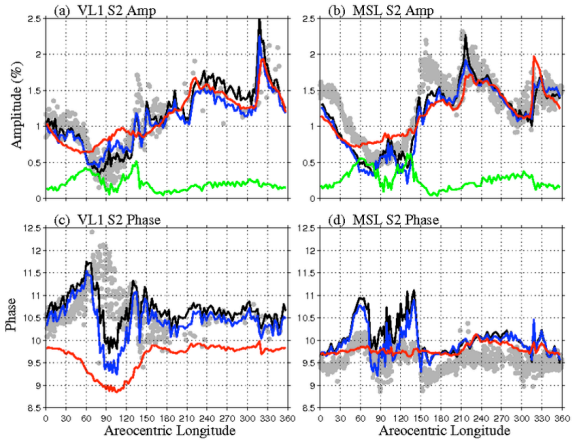

Figure 5. As for 4, but for the semidiurnal tide. The green curves show the contribution from SE2. The blue curves show the reconstruction of S_2 based on SW2 and SE2.

LMD simulations vs MSL and VL1: The ability to characterize the pressure response to the slope-wind circulation in Gale crater provides a means of isolating the planetary-scale thermal tide for comparison with observations at VL1 and with MGCM simulations. In Figs. 4 and 5, we show the simulated S_1 and S_2 amplitudes and their phases at VL1 and MSL from the LMD MY26 simulation. It is important to note that the comparison of the amplitude of simulated and observed S_1 is significantly improved by the elimination of the residual pressure signal in Gale crater (Gale crater is not sufficiently resolved in the LMD model, so there is no effect from a crater circulation). Although this simulation is in general agreement with observations, there are notable differences that are likely diagnostic of deficiencies in the formulation of thermal forcing in the models. These include the daily variation of water ice clouds and the possible influence of detached dust layers.

The resynthesized lander tide variation (in blue) based only on DW1 and DE1 accounts for much of the variability in the simulated S_1, while SW2 and SE2 together account for the S_2 signal. The synchronized decline in S_2 at VL1 and MSL is due to the combined impact of SW2 and SE2. This simplification, that closer agreement between simulations and observations may be achieved by changes to a very small number of tide modes, which are particularly responsive to planetary scale aerosol distributions, also suggests the possibility that a relatively small network of surface observation sites may be sufficient to gain a level of success in relating the observed tide response to thermal forcing.

References

Guzewich, S.D., et al. (2016), Atmospheric tides in Gale crater, *Icarus, 268*, 37-49, http://dx.doi.org/10.1016/j.icarus.2015.12.028.

Madeleine, J.-B., F. Forget, E. Millour, T. Navarro, and A. Spiga (2012), The influence of radiatively active water ice clouds on the Martian climate, *Geophys. Res. Lett., 39,* L23202, doi10.1092/2012GL053564.

Rafkin, S.C.R., et al. (2016), The meteorology of Gale Crater as determined from Rover Environmental Monitoring Station observations and numerical modeling. Part II: Interpretation, Icarus http://dx.doi.org/10.1016/j.icarus.2016.01.031.

Tyler, D. and J.R. Barnes (2013), Mesoscale modeling of the circulation in the Gale crater region: An investigation into the complex forcing of convective boundary layer depths, MARS 8, 5-177, doi:10.1555/mars.2013.0003.

Tyler, D., and J.R. Barnes (2015), Convergent crater circulations on Mars: Influence on the surface pressure cycle and the depth of the convective boundary layer, *Geophys. Res. Lett.*, 42, 7343–7350, doi:10.1002/2015GL064957.

Tyler, D., et al. (2017), Topographic circulations on Mars: Surface pressure, convective boundary layers and network implications, Sixth International Workshop on the Mars Atmosphere: Modeling and Observations, Granada, Spain, Jan 17-20, 2017.

Wilson, R.J., and K.P. Hamilton (1996), Comprehensive model simulation of thermal tides in the martian atmosphere, *J. Atmos. Sci*. 53, 1290-1326.

Wilson, R.J., S.R. Lewis, and L. Montabone (2008), Influence of water ice clouds on Martian tropical atmospheric temperatures, *Geophys. Res. Lett., 35*, L07202, doi:10.1029/2007GL032405.

Wilson, R. J., and S. D. Guzewich (2014). Influence of water ice clouds on nighttime tropical temperature structure as seen by the Mars Climate Sounder, *Geophys. Res. Lett.*, *41*, doi:10.1002/2014GL060082.

Zurek, R.W. (1976), Diurnal tide in the Martian atmosphere. *J. Atmos. Sci*., *33*, 321-337.